THEORETICAL METHOD OF THE OPTIMUM DESIGN OF A SUPERCAVITATING PROPELLER BLADE WITH SPOILER MOUNTED ON THE TRAILING EDGE

Zaw Win, G M Fridman and **A S Achkinadze,** St. Petersburg State Marine Technical University, Russia
(DOI No: 10.3940/rina.ijme.2010.a1.168)

SUMMARY

This paper presents theoretical design method to obtain 2-D optimum section with spoiler mounted on the trailing edge of a supercavitating propeller blade. Matched Asymptotic Expansions (MAE) is applied to determine the geometry of profile and cavity shape in the framework of potential flow theory. The blade section is of wedge-like shape and the opened cavity closure scheme is adopted. A typical section, on which the optimum blade design will be based, is singled out among the best individual sections from root to tip. The spoiler length of each hydrofoil section resulting from MAE method are finalized with CFD method so as to consider viscous effect under the same lift condition, others hydrofoil geometries being kept constant. The hydrodynamic performances of all blade sections being designed on the basis of the resulting typical section from linearized method are finally predicted with CFD method

NOMENCLATURE

D Propeller diameter (m)
V_s Ship speed (knots)
V_a Speed of advance (m sec^{-1})
V_r Resultant inflow velocity (m sec^{-1})
N Rotational speed (rpm)
V_∞ Inflow velocity (m sec^{-1})
V_0 Velocity of the free stream flow on the cavity (m sec^{-1})
V_1 Velocity on the boundary of stagnation zone in spoiler vicinity (m sec^{-1})
R_n Reynolds number
M Degree of polynomial equation
C_P Pressure coefficient
C_D Drag Coefficient of a hydrofoil
C_L Lift Coefficient of a hydrofoil
C_F Frictional resistance coefficient
J Advance coefficient
Q_s, Q_b Hydrodynamic fineness
K_D Delivered power coefficient of a blade
K_N Thrust power coefficient of a blade
T Operating temperature (^{o}C)
Z Blade number
b Blade span (m)
l Chord length of hydrofoil section(m)
n Rotational speed (rps)
p_0 Operating pressure (Pa)
p_v Vapour pressure (Pa)
t_i Thickness fraction
np Number of stations of a blade section
k Form index of the upper blade contour
w_s Wake fraction
ρ Density (kg m^{-3})
ν Kinematic viscosity (m^2 sec^{-1})
L Cavity length (m)
α Angle of attack (deg)
β Inclination angle of the spoiler (deg)
δ Maximum thickness fraction
σ Cavitation number
$\bar{\varepsilon}$ Relative spoiler length to chord
β_1 Pitch angle (deg)

1 INTRODUCTION

Supercavitation is the final state of cavitation. In this regime, the pressure in cavitating area is low and a big fixed cavity is formed. Compared with other types of cavitation, the interface of a supercavitation cavity is stable. Based on the potential flow analysis, Chaplygin [1] was the first to propose and analyze a new model of the free streamline flow past a flat plate with a region of constant pressure and the velocity V_0 on its boundary being slightly more than the inflow velocity V_∞ $V_0 = V_\infty\sqrt{1+\sigma}$, where cavitation number is $\sigma \geq 0$. All of numerical studies are based on the same 2-D physical model, where the pressure in a supercavitating cavity is uniform and equals to the vapour pressure. The interface of the cavity coincides with a streamline, and is smooth. Since then the conclusion was verified in numerous papers, reference to which can be found in classical books on the theory of jets in an ideal fluid by Gurevich [2] and Terentev [3], etc. It is notable that the model of stagnation zone is effective in free surface flow problems for planing and cavitating 2D and 3D hydrofoils with spoilers (fixed flaps of a very small relative to chord length). Achkinadze and Fridman [4] introduced such a new-type supercavitating hydrofoil by using the exact solution to the nonlinear flow problem. It is a wedge-like one with double-sided wetted parts, a short upper part and a long lower part. The upper part can be seen only in the vicinity of the leading edge and a lower is either flat or curvature with spoiler mounted on its trailing edge. In this paper, the length of the upper wetted part was taken into account to be very small in compare with chord. Matched Asymptotic Expansions (MAE) was applied to determine the geometry of profile and cavity shape in the framework of linear theory, Rozhdestvensky and Fridman [5]. The following steps were carried out to achieve the optimum hydrofoil for a supercavitating propeller by means of viscous-inviscid interactive method:

(a) The initial parameters were set up for the desired propeller and flow past the blade.

(b) The appropriate numbers of radial stations were assigned from root to tip of a blade.

(c) Local cavitation numbers were derived from the initial parameters for the different radial stations of the blade.

(d) Linearized MAE method was utilized to determine lower curvature, the angle of attack and the relative spoiler length, which ensures to attain minimum drag coefficient for every section, based on its local cavitation number. As a result, the best hydrofoil sections can be obtained for every station.

(e) Of all the best sections derived from MAE, one section was designated as a typical section of the blade first. Then profiles of other sections were generated from the basis of its lower curvature regardless of spoiler length. Maximum lift and minimum drag coefficient for such sections were also evaluated at the corresponding angle of attacks and local cavitation number σ_r. After that, the hydrodynamic fineness of an entire blade was derived. Hereafter it will be defined as blade-wise hydrodynamic fineness. Similarly all other sections were assigned as typical sections in turn and corresponding hydrodynamic fineness values are listed in a tabular form.

(f) The resulting blade-wise hydrodynamic fineness values derived from different typical sections were compared with each other. Among them, one section, which has maximum hydrodynamic fineness, was finally singled out as an optimum section of the blade.

(g) The spoiler length of all hydrofoil sections of a blade needs to be adjusted through CFD code, all other geometries and their lift coefficients being kept constant. Then the hydrodynamic characteristics are finalized with CFD method.

The authors have also developed a program to attain the optimum sections based on linearized potential flow theory. RANSE solver of Fluent was applied to consider viscous effect. Thus the present method can be used as one of the viscous-inviscid interactive methods because the optimization with linear theory assures to provide almost exact solutions and takes a few moments. Then spoiler correction solely needs to be performed by CFD method.

2 STATEMENT OF INVISCID FLOW PROBLEM WITH LINEARIZED THEORY

2.1 PROBLEM FORMULATION

Let us consider two-dimensional supercavitating hydrofoil operating in inviscid flow. The hydrofoil and cavity brings small perturbations into inflow. Therefore, linearization procedure has to be accomplished for nonlinear boundary condition both on free surfaces and

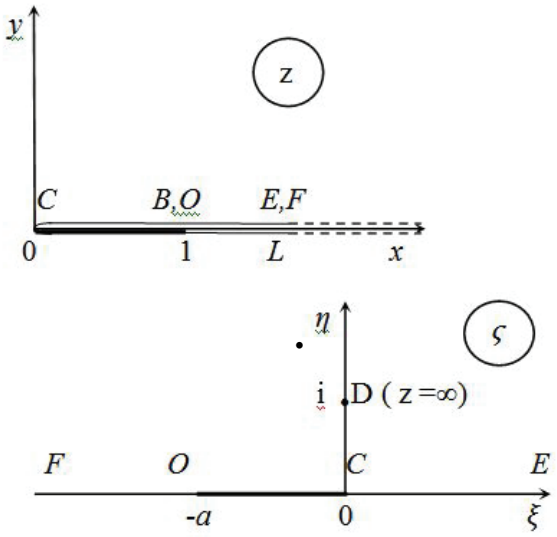

Figure 1: Physical and auxiliary planes

$$z = L\frac{\varsigma^2}{1+\varsigma^2} \qquad \varsigma = \sqrt{\frac{z}{L-z}} \qquad \alpha = \frac{1}{\sqrt{L-1}}$$

on the wetted portion of the foil [5]. The origin of the Cartesian coordinate system is taken at the plate's leading edge, x–axis being directed downstream and y upwards, see figure 1. All the wetted surface of the hydrofoil and the cavity appears as a slit of length L in the linearized plane $z = x + iy$, where L actually is a linearized cavity extent. Boundary conditions for real and imaginary parts of the conjugate velocity $\chi(z)$ are projected on the upper and lower boundary, see figure 1.

$$\chi(z) = u + iv = \frac{dw}{v_\infty dz} \tag{1}$$

and the complex potential function

$w(z) = \varphi + i\psi$,

The simple non-quadrature approach can be proposed for a wide range of functions $y = f(x)$ characterizing the lower surface distribution of the hydrofoil. It is obvious that the new function,

$$\Omega(z) = \chi(z) - 1 + i\theta(z)$$

where $\theta(x) = f'(x)$ is a tangential angle to the foil at point x, has pure real values on the wetted portion (as $x\varepsilon$ [0; 1], y = 0^+) and pure imaginary values on the cavity surfaces, see figure 1. Let us assume that the wetted portion of the cavitating hydrofoil is a polynomial

$$f(x) = 4hx(1-x) - \alpha x + x(1-x)\sum_{i=1}^{M} a_i x^i \tag{2}$$

where α is the angle of attack and h and a_i are polynomial coefficients.

Then function $\Omega(z)$, where $z = L\frac{\varsigma^2}{1+\varsigma^2}$, has to satisfy homogeneous boundary conditions on the upper semiplane ς in ∞ - ∞ class. It should be pointed out that the multiplicity of a pole at the infinity $z \to \infty$ for the function $\Omega(z)$ is equal to $(M+1)$, i.e. to the degree of the polynomial $f'(x)$. That is why the solution can be derived without an integration procedure and is of the form

$$\chi(\varsigma) = 1 - i\theta(z(\varsigma)) + \frac{iB}{\sqrt{\varsigma(\varsigma+a)}} + i\sqrt{\frac{\varsigma+a}{\varsigma}} \left\{ Im(A)\varsigma + Re(A) + \sum_{k=1}^{M+1}\left(\frac{C_k}{(\varsigma-i)^k} + \frac{\overline{C_k}}{(\varsigma-i)^k} \right) \right\} \quad (3)$$

where A and C_k, $k = 1,\ldots..,\ M+1$ are complex unknowns and B is a real parameter unknown as well.
Condition at infinity $z = \infty$ and at its image $\varsigma = i$ for function $\chi(\varsigma)$

$$\lim(\varsigma \to i)\ (\chi(\varsigma)) - 1) = \sigma/2 \quad (4)$$

$$\lim_{\varsigma \to i}\left\{ \chi(\varsigma) - 1)(\varsigma - i)^k \right\} = 0 \quad \text{for} \quad k = 1,\ldots.,M+1 \quad (5)$$

linearized cavity closure condition re-written in the form

$$Im\frac{dx}{d\varsigma}(i) = 0 \quad (6)$$

along with the matching condition allow unknown parameters A, B, C_k, and cavity extent L in (3) to be determined. Conditions (4) and (5) are complex what provides (2M+4) real conditions. Condition (6) and that from the matching give two additional real conditions.
So, the number $2M + 6$ of *real* unknowns coincides with that of *real* conditions. This solution scheme is correct in the case of the closed cavity closure model. In the further calculations we decide to adopt so called Wu-Fabula open cavity closure scheme which assumes a semi-infinite wake instead of the trailing edge of the cavity. Mathematically this scheme is a special case of the presented formulae (3)–(6). Indeed, one has to exclude the singularity at the trailing edge of the cavity as $x = L$ or $\varsigma = \pm\infty$. That is why $Im\ (A) = 0$ in formula (3) and condition (5) is valid no more. So, again, the number of unknowns $2M + 5$ is equal to the number of conditions.

The unknown real coefficient B can be found in the course of the matching procedure with so called inner asymptotic solution in the vicinity of the hydrofoil's trailing edge. In detail it was done, for instance, in [5]. The resulting expression for B is as follows:

$$B = -\frac{\beta}{\pi}\frac{\sqrt{L}}{L-1}\sqrt{\frac{\overline{\varepsilon}}{R}} \quad (7)$$

$$R = \int_0^1 \xi\left(\frac{1+\xi}{1-\xi}\right)^{\frac{\beta}{\pi}} d\xi$$

Finally, the following algorithm can be formulated for deriving all the unknowns in the problem.

- first, one has to use $M + 1$ complex conditions (4) which produce a homogeneous system of linear equations in $M + 1$ complex unknowns C_k. This system is readily solved;
- second, substituting all the coefficients C_k into the complex condition (5), one can get an expression for A. Condition $Im\ (A) = 0$ which holds in the case of the open cavity closure scheme is reduced to nonlinear equation in terms of the cavity length L only. The Newton's method enables one to obtain a numerical solution to the nonlinear equation and get the value for L and A as well;
- third, once L is known, the value of B is easily calculated from equation (7).

Once function $\chi(\varsigma)$ is found (i.e. all the unknowns are derived), the cavity volume is determined

$$y_{cav}^{+} = -Im\left\{ \int_0^{\chi} \chi\left(\sqrt{\frac{t}{L-t}} \right) dt \right\},$$

$$y_{cav}^{-} = -Im\left\{ \int_0^{\chi} \chi\left(\sqrt{\frac{t}{L-t}} \right) dt \right\} + f(1)$$

where superscripts + and – denote the upper and lower boundary of the cavity correspondingly.

All the hydrodynamic coefficients are also connected to $\chi(z)$

$$C_p(x) = -2Re\left\{ \chi\left(-\sqrt{\frac{x}{L-x}} \right) - 1 \right\} \quad (8)$$

$$C_L = \int_0^1 C_p(x)dx \quad (9)$$

$$C_D = \int_0^1 C_p(x)\theta(x)dx \quad (10)$$

Hydrodynamic fineness of a hydrofoil section Q_s will be:

$$Q_s = \frac{C_L}{C_{|D} + C_F} \quad (11)$$

where

$$C_F = 0.455/(Log\ R_n)^{2.58}$$

2.2 MAE PROGRAM OF HYDROFOIL SECTIONS

The authors created a program to obtain the foil section of the maximum hydrodynamic fineness based on initial data such as a length of cavity L, cavitation number σ, lift coefficient C_L, spoiler inclination angle β, polynomial equations with degree index M for lower contour of a foil. The angle of attack α, spoiler length ε, drag coefficients C_D, hydrodynamic fineness Q_s and polynomial coefficients of a lower contour of the foil are comprised of a program output. Such a program includes

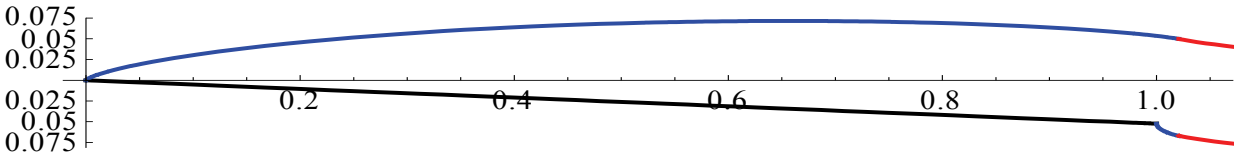

Figure 2: Cavitating flow with the parameters; $\sigma = 0.35$, $\alpha = 3^o$, $\beta = 90^o$, $\varepsilon = 0.01$, $L = 1.02$

the option so that one can choose the upper contour, wedge-like or half parabolic or parabolic segment, before running the program. Since it is necessary to adjust thickness near the leading edge from the viewpoints of strength and production, the authors created the new expression, namely thickness distribution, for such three types of upper contour as the variants of standard functions. The half parabolic segment can be defined as:

$$t_i = t_s^k t_{T.E} \qquad (12)$$

where

t_i = modified relative thickness to $t_{T.E}$

t_s = standard relative thickness at each station along the chord

$t_{T.E}$ = relative thickness to chord at the trailing edge

k = form index

In the above equation, k and $t_{T.E}$ vary in the blade radial stations, based on strength criteria of a blade. Most of $t_{T.E}$ can be found as maximum thickness fraction δ of the blade sections but for some of sections, especially near the blade tip, the maximum thickness fraction δ may not coincide with $t_{T.E}$ to avoid very thin leading edge. Leading edge thickness can be controlled by varying form index k of contour about ±0.3. Besides, it is necessary to know reliable thickness distribution along the radial axis of a blade because there are no criteria to check the blade strength in the program. Therefore, the maximum thickness to chord ratio δ of a section is an input data of the program as $t_{T.E}$. Moreover, it is necessary to predict the length of cavity in accord with practical working condition.

The main task of program is to find the blade with optimum hydrofoil section at all radial stations for the given set of input parameters mentioned above. In doing so, the condition is set up to meet basic requirements that the foil has to inscribe in the fixed big cavity, i.e. the free streamline can touch the upper contour of the blade but must not intersect each other. The algorithm is created in two different purposes. The fist part of the program intends to find lower contour of the blade section, i.e. to derive the polynomial coefficients. In that case, lift coefficient is a main input but the condition may fail if it is unrealistic. If so, input parameters including lift coefficient have to be replaced with new entries until conditions pass successfully. The second part is to find the parameters for the other sections on the basis of the lower face with the polynomial coefficients resulting from the first part of program. It should be noticed that the comparison of Q_s is very important in any iteration. If one finds the message of failed conditions, lift coefficient C_L needs to be decreased for the first part of the program and spoiler length ε to be reduced for the second part. On the other hand, if the program is still passing the conditions of the minimum C_D , one can increase C_L for the first part and extend the spoiler length ε for the second part so as to achieve maximum Q_s. For instance, we can see flow model comprising a upper cavity (blue), a lower wetted part of the foil (black) and semi-infinite wake (red) in figure 2. Figure 3 depicts Graphical User Interface (GUI) of MAE program.

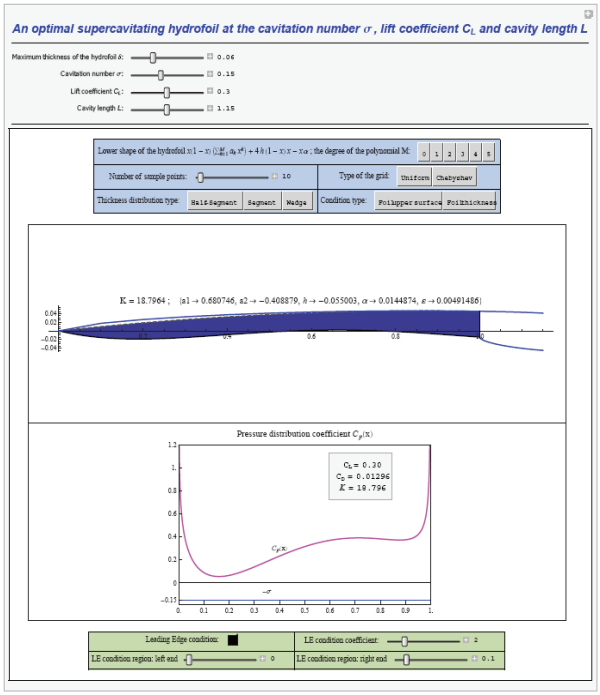

Figure 3: MAE program (GUI)

3 STATEMENT OF VISCOUS FLOW PROBLEM WITH CFD

The importance of CFD in cavitation prediction has been increasing. The current multi-phase flow capabilities of some of the more advanced Reynolds Averaged Navier–Stokes (RANS) solvers are being found to be helpful in gaining insights into the cavitation performance viscous-inviscid interactive methods of marine propellers [6]. Therefore, the resulting inviscid model of linear flow problem can be checked by any computational fluid dynamics (CFD). In this paper, the modeling of the viscous flow past the SC foil was carried out by means of RANS solver of FLUENT when the meshing is complete

in GAMBIT. The turbulent model is Spalart-Allmaras (S-A). The analysis of fluid dynamics was carried out thoroughly in [9]. As a result, linear solutions agreed with CFD if one can properly adjust only spoiler length. Here, for instance, the authors presented a solution to a cavitating flow problem by means of viscous/inviscid interactive method.

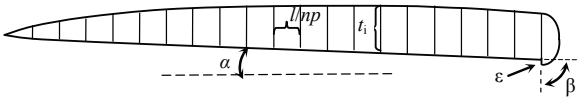

Figure 4: 2-D Hydrofoil resulting from MAE method

First of all, as shown in figure 4, it is necessary to configure the body consisting of the lower wetted surface of the foil including spoiler, the upper cavity surface in GAMBIT. Then the suitable boundary conditions are defined in FLUENT. The mesh elements need to be created about 408000 including boundary sub layer nearest to wall with minimum cell thickness, y_p of 0.003 mm. One can determine the minimum cell thickness by using the equation in [8].

$$y_p = y^+ \nu \Big/ \left(u_\infty \sqrt{(C_f/2)}\right) \tag{13}$$

Where $y^+ > 30$ or $y^+ < 5$,

Frictional resistance coefficient C_f is derived from Reynolds Number.

$$\frac{C_f}{2} = 0.037 R_n^{-\frac{1}{5}} \tag{14}$$

where

$$R_n = u_\infty \frac{l}{\nu}$$

The cavitating flow model is set up under the following operating conditions [6] &[14];

Fresh water temperature, T	- 15°
Density of water, ρ	- 999
Kinematic viscosity of water , ν	-1.14 x 10^{-6}
Density of water vapour, ρ	- 0.013
Kinematic viscosity of water vapour, ν	-7.15 x 10^{-4}
Saturated vapour pressure p_v	- 1700

At the inception of calculation, the type of flow is set up as a single- phase steady flow. The iteration is complete when the convergence of continuity equation reaches to the value of 10^{-5}, which is one of the convergent criteria of the residuals. The numbers of iteration were generally undertaken about 3500. Then the flow type has to be changed as multi-phase unsteady flow and the cavitation mode is turned on to consider the cavitation. In post-processing, the lift coefficient in CFD is compared with that of linear solution. If the former is less than the latter, the spoiler length has to be lengthened to some extent, the other parameters being kept constant. Then the iterations are repeated in the procedure mentioned above until lift coefficient is identical between two methods. After completion of iterations, one can check the pressure distributions and wall y^+ distributions on the surfaces, velocity and total pressure contours in the whole domain. The figure 5 shows that the wall y^+ distribution on hydrofoil and cavity. The y^+ is defined as $y^+ = \frac{u_* y}{\nu}$ where u_* is frictional velocity near wall.

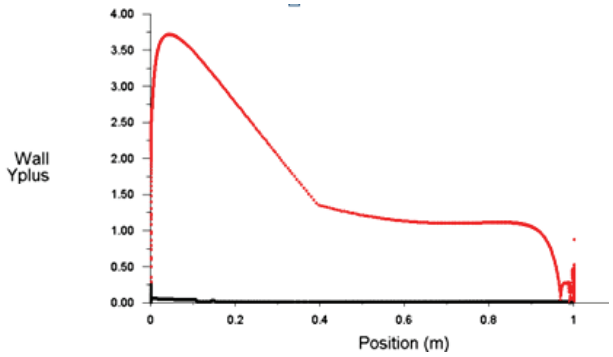

Figure 5: The wall y^+ distribution on hydrofoil (red) and cavity (black) for the set of parameters; $\sigma = 0.35$, $\alpha = 3^o$, $\beta = 90^o$, $\bar{\varepsilon} = 0.01$

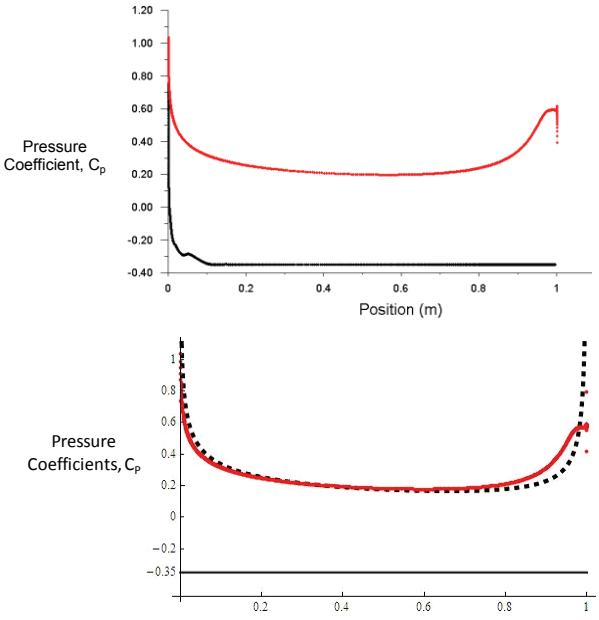

Figure 6: (a) CFD (b) Comparison of pressure coefficient distribution between CFD & LT; C_P on the wetted side - CFD (red) & LT (black dashed) and cavity side (black solid) for the case of $\sigma = 0.35$, $\alpha = 3^o$, $\beta = 90^o$, $\bar{\varepsilon} = 0.01$

The figure 6 depicts the distribution of pressure coefficients on the lower part of hydrofoil and cavity, compared LT with CFD. It can obviously be seen that the pressure coefficient on the boundary of the cavity is equal to negative cavitation number, i.e $C_p = -\sigma$

4 VERIFICATION OF CFD CODE FOR CAVITATING HYDROFOIL

4.1 EXPERIMENTAL DATA

The hydrofoil model as shown in figure 7 has a 7.62 mm chord and 7.366 mm span. The coordinates of the profile, as specified by the David Taylor Model Basin, can be obtained in [10].

Figure 7: Profile of model hydrofoil

Figure 8: Typically recorded photographs,
V = 30 fps, α= 5°
(a) σ_v = 1.604, V= 30.7 fps (b) σ_v = 0.657, V=30.9 fps

The experiments were conducted in the two-dimensional test section of the High Speed Water Tunnel. During the tests the water temperature varied between 23.67°C and 25°C**.** The vapour pressures of water for these temperatures are 2896 and 3171. The air content of the water, as measured with a Van Slyke gas content analyzer, was approximately seven parts of air per million parts of water throughout the tests. The measured cavity pressure for vapour cavitation was approximately 3447. The excess pressure above vapour pressure of the water was caused by diffusion of air into the cavity. Because of the thinness of the hydrofoil, sizeable deflections occurred under hydrodynamic loading. Since it was impractical to compute this angular twist from the hydrodynamic forces, the deflections were determined experimentally for each data point by means of a cathetometer telescope mounted outside the test section window. Vibration of the leading edge of the foil often made it impossible to make accurate measurements at the leading edge; therefore, a third measurement near the centre of the model chord, where there was essentially no vibration, provided twist data which were also accurate to ±0.05°. Photographs of the cavitating hydrofoil were taken at each data point. As shown in figure 8 typical examples of these pictures were taken with a 1/30-second exposure and shows the extent of the cavitation on the hydrofoil.

4.2 NUMERICAL RESULTS FROM CFD CODE

First of all, a 2D section is created in GAMBIT as the coordinates of the profile described in [10]. There are about 300000 cells in flow domain. Then RANS solver, FLUENT, is chosen and the necessary boundary conditions are set up in pre-processing in account with Waid[10]. Spalart-Allmaras (S-A) is applied as a turbulent model. The cavitating flow problems are generally solved in two steps, first in single phase flow and secondly in two phase flows. That is why the cavitating flow problems should be solved after having obtained the reasonable pressure fields around the foil. Single phase flow needs to be converged until the residual of momentum equation is below 10^{-6} . In the first step, the boundary conditions of the flow domain are taken into account with velocity inlet and outflow scheme. After convergent of single phase solution, boundary condition has to be changed with a pair of velocity inlet and pressure outlet and the cavitation mode is turned on. As for second step, the solutions will be reasonable when all of residual are below 10^{-3}. Steady segregated solver is used at single phase flow but unsteady solver is suitable for multi-phase flow. The figure 9 demonstrates cavity shape at two cavitation numbers, σ_v = 1.604, σ_v = 0.657. The comparison of lift and drag coefficients can be found in as follows;

σ	Experiment data		CFD	
	C_L	C_D	C_L	C_D
1.604	0.599	0.0449	0.6065	0.04432
0.657	0.811	0.0501	0.8084	0.05109

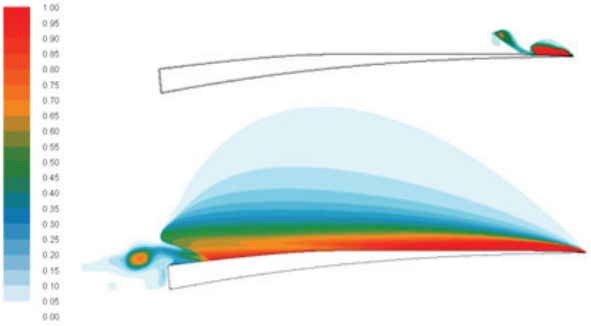

Figure 9: Contours of water vapor fraction around hydrofoil

5 METHOD OF OPTIMUM BLADE DESIGN WITH LINEARIZED THEORY

5.1 FORMULATION OF HYDRODYNAMIC CHARACTERISTICS OF A PROPELLER BLADE

The term ‘propeller design basis’ refers to the power, rotational speed and ship speed that are chosen to act as the basis for the design of the principal propeller

geometric features. An optimum blade should have good agreement with such a requirement that it demands least power to reach the design speed in the reasonable range of rotational speed. To meet this aim, it is necessary to select the blades of maximum hydrodynamic fineness.

Let us consider the delivered power of a 2-D hydrofoil section as shown in figure 10 to overcome total drag force along the direction of resultant inflow velocity V_r.

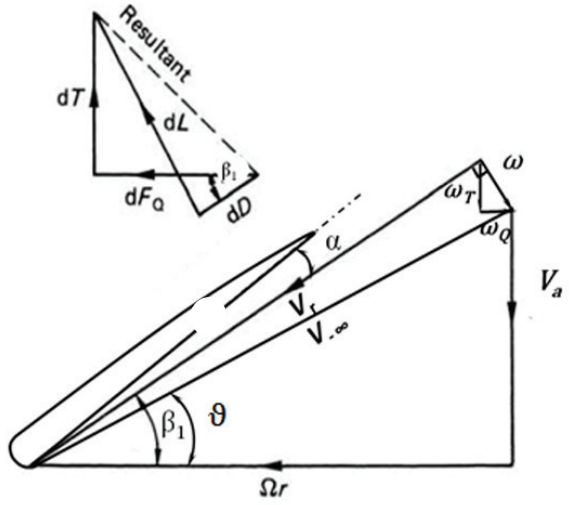

Figure 10: Vector diagram of inflow velocity

$$\Delta P_{D_r} = R_T V_r$$

For an entire blade,

$$P_{D_b} = \sum_{r=1}^{n} \Delta P_{D_r} = \int_{r_1}^{r_n} \frac{1}{2} \rho C_T b V_r^3 dr \tag{15}$$

Power coefficient K can be obtained from the following relationship,

$$K = \frac{P}{\rho n^3 D^5} \tag{16}$$

Delivered power coefficient K_D of a blade is derived from equation (15) & (16)

$$K_D = \frac{1}{4} \int_{\bar{r}_h}^{1} C_T \frac{b}{D} \left(\frac{v_R}{nD} \right)^3 d\bar{r} \tag{17}$$

Where $\bar{r} = \frac{r}{R}$, $\bar{r}_h = \frac{r}{R}$ at the blade root,

$$C_T = C_D + C_F$$

Besides, $J = \frac{V_a}{nD}$,

$$v_r = \sqrt{(v_A + \omega_T)^2 + (\Omega r - \omega_Q)^2}$$

Similarly lifting power of a 2-D hydrofoil section in the direction perpendicular to the resultant inflow velocity V_r is as follows:

$$\Delta P_{T_r} = F V_a \cos^{-1} \beta_1$$

For an entire blade,

$$P_{T_b} = \sum_{r=1}^{n} \Delta P_{T_r} = \int_{r_1}^{r_n} \frac{1}{2} \rho C_L b V_r^2 V_a \cos^{-1} \beta_1 dr \tag{18}$$

We have lifting power coefficient K_N of a blade from equation (16) and (18)

$$K_N = \frac{1}{4} \int_{\bar{r}_h}^{1} C_L \frac{b}{D} \left(\frac{v_R}{nD} \right)^2 J \cos^{-1} \beta_1 d\bar{r} \tag{19}$$

Thrust coefficient and torque coefficient of a propeller in [7] will be as follows;

$$K_T = \frac{Z}{4} \int_{\bar{r}_h}^{1} C_L \frac{b}{D} \left(\frac{v_R}{nD} \right)^2 \cos \beta_1 \left(1 - \frac{1}{Q_s} \tan \beta_1 \right) d\bar{r} \tag{20}$$

$$K_Q = \frac{Z}{8} \int_{\bar{r}_h}^{1} C_L \frac{b}{D} \left(\frac{v_R}{nD} \right)^2 \sin \beta_1 \left(1 + \frac{1}{Q_s} \cot \beta_1 \right) \bar{r}\, d\bar{r} \tag{21}$$

Hydrodynamic fineness of an entire blade Q_b will be;

$$Q_b = \frac{K_N}{K_D} \tag{22}$$

Open water efficiency η_D will be;

$$\eta_D = \frac{K_T}{K_Q} \frac{J}{2\pi} \tag{23}$$

5.2 PROGRAM FOR OPTIMUM BLADE DESIGN

The main program of the optimum blade design is created on the basis of ship speed, propeller diameter and propeller revolution. Those parameters depend on hull design. That is why the propeller selection is carried out when designer has already determined the appropriate hull form which ensures to achieve the designed speed. Therefore the diameter of a propeller may have a limit to achieve the desired speed, especially high-speed craft. Furthermore propeller revolution also corresponds to propulsion engine. High-speed small craft needs small engine of high weight power ratio and most of them are high speed engines. As a result, it is necessary to install the propeller of small diameter with high revolution. Such requirements contribute to develop supercavitating propeller. However there are some drawbacks of supercavitating propeller so far. Hence water jet propulsion is dominant in high-speed light craft. The method mentioned in present paper may fulfill those requirements to some extents.

First of all one has to set up the initial parameters such as ship speed, wake fraction, diameter of propeller, number of revolutions, density and kinematic viscosity of water and watervapour, depth of the propeller centerline under water surface. According to those data, the local cavitation numbers, Reynolds numbers and frictional resistance coefficients at each radial station can be derived from first subroutine program. Such parameters are input data of MAE program, which is second subroutine program. Then the output of MAE program

consisting of section-wise hydrodynamic fineness, lift and drag coefficients are the input data of former program again to find blade-wise hydrodynamic fineness and open water efficiency. All blade sections have to be considered as a typical section of a blade and collected blade-wise hydrodynamic fineness of each typical section. After compared those coefficients, one needs to single out the blade section of maximum coefficient Q_b. It is the most optimum typical section of all sections.

6 NUMERICAL RESULTS

The viscous-inviscid interactive methods with different approaches have already introduced to predict sheet cavitation of a propeller by Sun and Kinnas [6]. In their approach the inviscid wetted and cavitating flows are analyzed using a low-order potential boundary element analysis based on a thin cavity modeling approach. Then by making the assumption of two dimensional boundary layer acting in strips along the blade, the effects of viscosity on the wetted and cavitating flows are taken into account by coupling the inviscid model with a two-dimensional integral boundary layer analysis procedure. The method in present paper can also be used one of the viscous-inviscid interactive methods.

A sample blade design was also carried out in this paper. First of all, the desired propeller blade and its operating conditions were set up.

Propeller revolution, N	1465
Diameter, D	1.054
Ship speed, V_s	63
Wake ratio, $(1\text{-}w_s)$	0.95 (assumed)
Number of blades, Z	3

Furthermore, thickness distributions and blade span at all radial stations should be known in advance, see table1. In the present paper, those are quoted from the proven propeller of different type.

Table 1: Thickness distributions and blade span ratio

r/R	$t_{T.E}$	b/D
0.3	0.1012	0.564
0.4	0.0615	0.719
0.5	0.0405	0.844
0.6	0.0277	0.929
0.7	0.019	0.967
0.8	0.0122	0.947
0.9	0.0087	0.781
0.95	0.0082	0.547
1		

6.1 RESULTS FROM LINEARIZED THEORY

Before commencing the program, the initial data were set up as follows;

Cavity length (open model), L	= 1.15
Polynomial index, M	= 2
Spoiler inclination angle, β	= 90°
Number of station, np	= 20

Although the above variables are constant for all sections, local cavitation number σ_r, form index k, thickness $t_{T.E}$, frictional resistance coefficient C_F which can be derived from equation (11), need to be set up for individual hydrofoil. Form indices for sample design are shown in table 2.

Table 2: Form index k of a sample blade

r/R	k
0.3	0.2
0.4	0.15
0.5	0.05
0.6	-0.1
0.7	-0.2
0.8	-0.27
0.9	-0.3
0.95	-0.31

Then one can run the optimization program. For present blade design, seven typical sections were chosen to obtain the best one in present case. Such sections correspond to seven radial stations from TS1 to TS7.

Table 3: Section-wise hydrodynamic fineness Q_s

r/R	σ_r	TS1	TS2	TS3	TS4	TS5	TS6	TS7
0.3	0.130	13.41	12.92	13.13	12.92	12.65	12.53	12.50
0.4	0.100	18.28	18.78	18.41	18.51	18.56	18.20	18.27
0.5	0.077	21.65	22.33	22.47	21.97	22.24	21.92	22.10
0.6	0.061	21.59	20.14	23.72	24.55	24.09	23.73	21.41
0.7	0.048	19.08	18.40	21.41	22.44	24.82	22.03	19.84
0.8	0.039	20.58	20.06	23.75	23.83	23.82	24.56	21.56
0.9	0.032	19.90	20.77	19.64	20.93	21.02	21.58	22.37
0.95	0.029	17.15	18.47	18.21	18.36	18.63	19.38	19.86

The optimization program evaluated the hydrodynamic fineness Q_s for all sections, see table 3. It is obvious that each typical section has maximum Q_s at its radial stations, r/R. Hence there are seven types of blade to be selected on the basis of their hydrodynamic fineness Q_b.

Table 4: Blade-wise hydrodynamic fineness Q_b

	K_D (x 10^3)	K_N	Q_b
TS1	8.94	0.1102	12.32
TS2	9.20	0.1122	12.19
TS3	8.63	0.1132	13.12
TS4	8.51	0.1141	13.40
TS5	**8.42**	**0.1147**	**13.63**
TS6	8.64	0.1155	13.36
TS7	9.05	0.1150	12.69

As compared Q_b in table 4, section TS5, which lies at the radius of the 0.7 R, is the most optimum typical section of an entire blade. MAE program generated the following polynomial coefficients of the lower contour of the blade sections from equation (2);

M =2, h = –0.018, a_1 = 0.196, a_2= – 0.141

Finally, one can draw general outline of the blade sections, see figure 11.

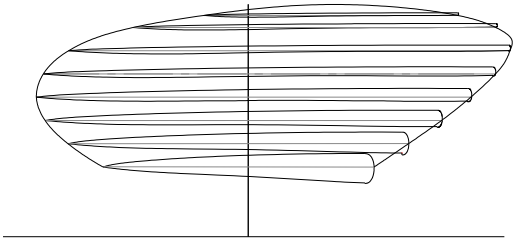

Figure 11: General outline of resulting optimum blade section from linear theory

6.2 RESULTS FROM CFD CODE

After completion of linearized method, it is necessary to consider the viscous flow model so as to lengthen the resulting spoiler from linear theory. As mentioned in previous section (3), all of the blade sections were verified by FLUENT to make spoiler length correction because of the stagnation zone in the vicinity of spoiler that omitted to be take into account in linearized method. In doing so, the hydrodynamic characteristics of some of the optimum blade sections resulting from such method need to be compromised a little so as to ensure smooth variation of the spoiler length from root to tip. Moreover, the hydrofoil geometry and its characteristics have been finalized for entire blade as shown in table 5. It is obvious that the coefficients of hydrodynamic fineness in table 5 are not quite different from those under TS5 in table 3. However there were small changes in hydrodynamic characteristics of the blade, i.e. delivered power coefficient K_D and thrust power coefficient K_N are 0.00904 and 0.1136 respectively instead of 0.00842 and 0.1147 in linear solution shown in table 4. Consequently hydrodynamic fineness of the blade Q_b decreased from 13.63 to 12.56. The open water efficiency η_D can also be derived from equation (23). Finally the desired supercavitating propeller was examined through CAD to view its surface fairness of the blade in three dimensions.

The characteristics of resulting propeller shown in figure 12 are as follows;

Diameter of propeller, D -	1.054
Propeller revolution, N -	1465
Blade Area Ratio, BAR -	1.085
Rake angle -	15°
Skew angle -	25°
Number of blade -	3
Direction of rotation -	left
P/D ratio (0.7 R) -	1.35
Cavitation number, σ -	0.21
Advanced coefficient, J -	1.2
Thrust coefficient, K_T -	0.175
Torque coefficient, K_Q -	0.042
Open water efficiency, η_D -	0.79

Table 5: The hydrodynamic characteristics of all sections of a blade resulting from CFD

r/R	σ_r	C_L	$\sum C_D$	Q_s
0.3	0.130	0.2412	0.0209	11.49
0.4	0.100	0.1902	0.0115	16.53
0.5	0.077	0.1500	0.0076	19.74
0.6	0.061	0.1178	0.0048	24.53
0.7	0.048	0.0889	0.0036	24.88
0.8	0.039	0.0752	0.0035	21.36
0.9	0.032	0.0623	0.0031	20.21
0.95	0.029	0.0544	0.0028	19.04

Figure 13 and 14 illustrate the variation of spoiler length from root to tip. The results from CFD reveal that the relative spoiler lengths to chord exist in the range of 0.001 to 0.005. CFD code demonstrates contours of the vapor fraction around the hydrofoil, see figure 15.

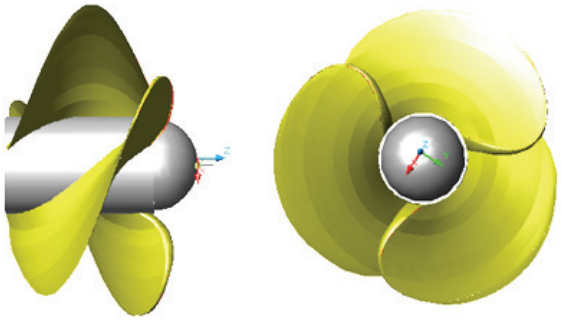

Figure 12: 3-bladed supercavitating propeller

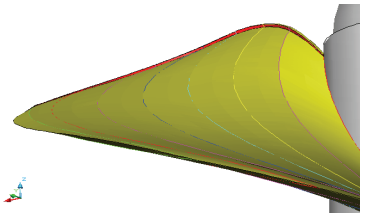

Figure 13: Spoiler (red) on the trailing edge

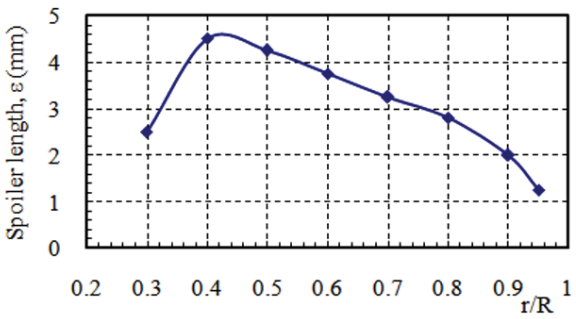

Figure 14: Spoiler length variation along the trailing edge

The red region is a cavity with full of water vapor. In figure, while one can only express the cavity length for closed cavity model, that of open model is physically implicit because linear theory defined it as a distance from leading edge to the point, behind which the semi-infinite wake appears in the same thickness of cavity.

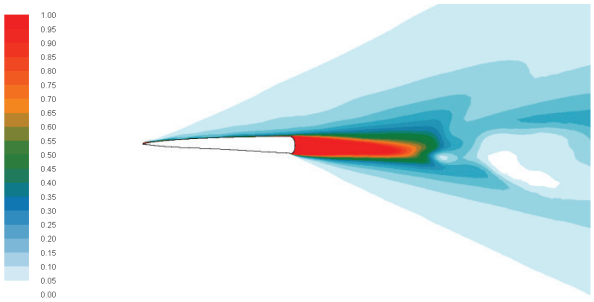

Figure 15: Contours of vapor fraction around the blade section of 0. 3 R

7 DISCUSSIONS

7.1 FACTORS AFFECTING THE OPTIMUM HYDROFOIL IN LINEARIZED THEORY

The hydrodynamic fineness for a given lift force is influenced by parameters consisting of the upper and lower curvature of a foil, the angle of attack α, the spoiler length ε, the inclination angle of spoiler β and the relative thickness δ of a foil. According to numerical results, the upper and lower surface curvature of a hydrofoil affect the hydrodynamic fineness to some extents, see figure 16. That is why the contour of free streamline over the hydrofoil depends on the cavitation numbers. Generally it can be divided into two types, wedge-like and parabolic. Wedge-like cavity on the hydrofoil occurs at a small cavitation number while parabolic shape appears at a larger cavitation number. One should have considered which types of upper contour of blade will be chosen so as to match the cavity being likely to appear on the hydrofoil since the inception of foil design.

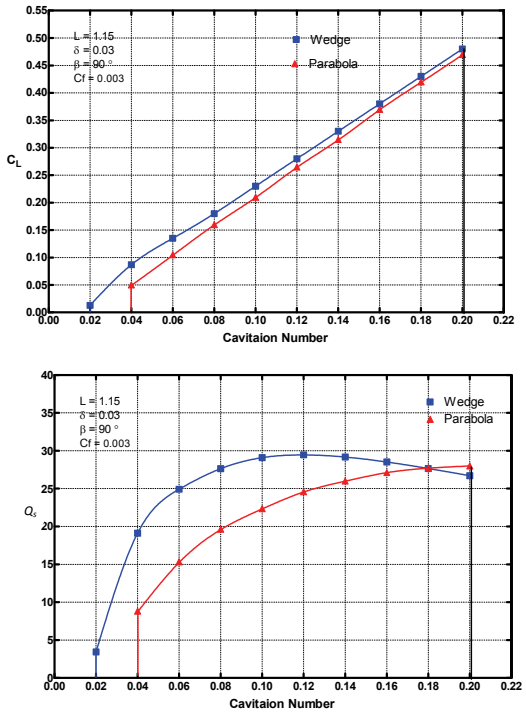

Figure 16: Comparison of C_L & Q_s between wedge-like and parabolic contour of upper face of a hydrofoil section

The choice of a lower contour of the blade section is a matter of the utmost importance as well. In present paper, the hydrodynamic performance analysis has been carried out by the MAE method as shown in figure 17. In doing so, lift coefficient was kept constant and thickness distribution was assigned as a half-parabolic segmental function.

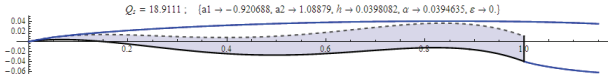

(a) Lower quartic polynomial contour without spoiler, $C_L = 0.33$, $\sigma = 0.15$, $L = 1.15$, $\delta = 0.05$, $\alpha = 2.26°$, $\bar{\varepsilon} = 0$, $Q_s = 18.911$

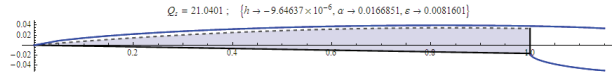

(b) Lower flat with spoiler, $C_L = 0.33$, $L = 1.15$, $\delta = 0.05$, $\sigma = 0.15$, $\alpha = 0.96°$, $\beta = 90°$, $\bar{\varepsilon} = 0.0082$, $Q_s = 21.040$

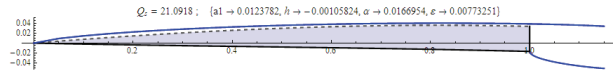

(c) Lower cubic polynomial contour with spoiler, $C_L = 0.33$, $\sigma = 0.15$, $L = 1.15$, $\delta = 0.05$, $\alpha = 0.96°$, $\beta = 90°$, $\bar{\varepsilon} = 0.0078$, $Q_s = 21.092$

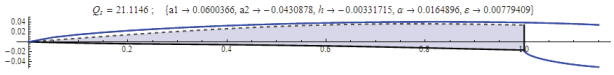

(d) Lower quartic polynomial contour with spoiler, $C_L = 0.33$, $\sigma = 0.15$, $L = 1.15$, $\delta = 0.05$, $\alpha = 0.95°$, $\beta = 90°$, $\bar{\varepsilon} = 0.0078$, $Q_s = 21.115$

Figure 17: Supercavitating flow past hydrofoil of four different types

It is noted that the lower face without spoiler shown in figure 17 (a) is the same as a hydrofoil section with pressure-side camber. As compared Q_s, the lower face of 4^{th} degree polynomial contour with spoiler renders the highest hydrodynamic fineness while hydrofoil without spoiler provides the lowest. As for higher 4^{th} degree,

there are no significant changes in hydrodynamic coefficients. In view of foil thickness, the hydrodynamic fineness of a thick foil is less than that of slender foil under the same condition.

7.2 SPOILER-LENGTH CORRECTION WITH CFD

The spoiler-length correction plays vital role of the viscous-inviscid interactive method in the present paper. That is why stagnation zone in front of spoiler causes the changes in direction of the streamline of fluid flow in the vicinity of spoiler. Stagnation zone appears due to viscous effect on the wetted surface of the lower part of the hydrofoil, see figure 18.

Figure 18: Velocity contours around the blade section of 0.5 R and stagnation zone in front of its spoiler

Since linearized method is taken into account without viscous effect, spoiler length resulting from such method is shorter than that obtained from CFD method. As a result, the relative spoiler lengths of blade sections were extended from 2.3 to 2.8 times of those resulting from linearized method in this case, see figure 19.

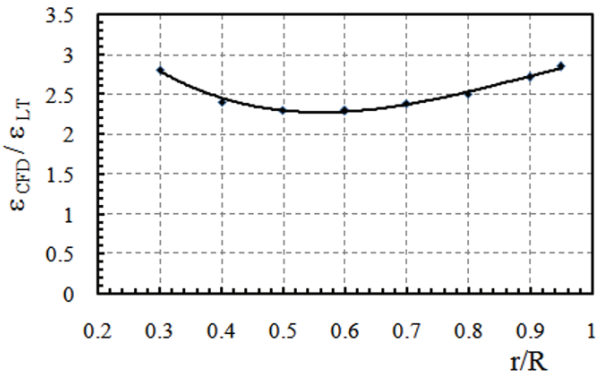

Figure 19: The spoiler ratio of CFD to linear theory along the radial direction

ε_{CFD} = Spoiler length resulting from CFD
ε_{LT} = Spoiler length resulting from linear theory

7.3 LEADING EDGE CORRECTION WITH CFD METHOD

The leading edge of the blade section resulting from MAE method is of sharp edge. The flow past such hydrofoil illustrates that the stagnation point cannot coincide with leading edge, i.e. the hydrofoil does not operate in shock-free mode, see figure 20. Therefore, it is necessary for all of blade sections to be made leading edge correction with CFD method as shown in figure 21. In doing so, the authors also created a program to obtain appropriate profile of leading edge in line with streamline flow on the base of cavitation number and angle of attack, modifying solving method to the local problem of free surface at leading edge (Plotkin Scheme)[16].

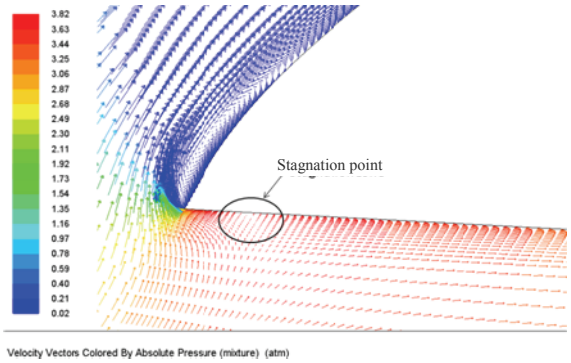

Figure 20: Blade profile without leading edge correction

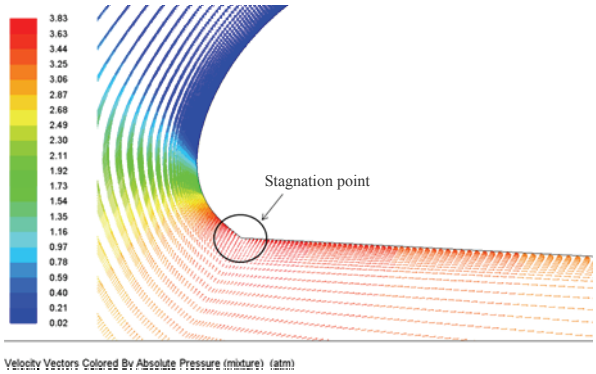

Figure 21: Blade profile with leading edge correction

8 CONCLUSION

As mentioned in the introduction, the effort in this paper is to achieve the optimum hydrofoils with spoiler mounted on the trailing edge of a supercavitating propeller. Numerical analysis was carried out rigorously to study factors affecting the hydrodynamic characteristic of the supercavitating hydrofoil. The geometry of optimum hydrofoil inscribed in the cavity was defined successfully by two steps. The first step is to predict the inviscid flow model around the hydrofoil in the framework of linearized potential flow theory. Such an approach is unable to consider an effect of the stagnation zone, which emerged in the vicinity of spoiler due to viscous effect. It influences the hydrodynamic characteristics to some extents. Therefore, as the second step, CFD method needs to be applied to finalize the foil geometry without any changes in its resulting geometry

from first approach except spoiler. In doing so, the length of spoiler has to be adjusted, lift coefficient being kept constant. Although the present approach needs to be carried out within a few moments, it is necessary to conduct some experiments in cavitation tunnel or open water propeller test. Unfortunately the authors can not submit experiment results in this paper but can verify Waid's section without spoiler in CFD code. Moreover, design consideration of the blade strength is beyond the scope of this paper. Hydrofoil thickness governs the cavity volume considerably since almost the whole surface of the upper part of foil should be free from liquid. The smaller the cavity volume, the higher the hydrodynamic fineness of a foil will be. Therefore, one should choose the material of high strength to produce thin and strong blade.

9 REFERENCES

1. Chaplygin, S.A. To the problem of jets in an incompressible fluid, *Trudy otdeleniya phys. nauk, vol. X, No. 1, Moscow (in Russian),* 1899.
2. Gurevich, M.I. The theory of jets in an ideal fluid, *Nauka Publ., Moscow (in Russian),* 1979, pp-536.
3. Terentev, A.G. Mathematical aspects of cavitation. *Chuvash State University, Cheboksary (in Russian)*, 1981, pp-131.
4. Achkinadze, A.S. & Fridman, G.M. Optimal sections for propellers with spoiler and preset leading edge angle. *Proceedings of the International Conference on Propeller Cavitation - NCT'50, University of Newcastle, Newcastle, United Kingdom*, April 3-5, 2000, pp-263-274.
5. Rozhdestvensky, K.V. and Fridman, G.M. Supercavitating nonlinear flow problems: matched asymptotics. *Supercavitating Flows, NATO - RTO Lecture Series 005, pp. 19(1)-19(30*, 2002.
6. Carlton, J.S. (2007). Marine Propellers and Propulsion, *2nd ed. Elsevier Ltd.,* 2007.
7. Artushkov, L.C., Achkinadze, A.S. and Russetskiy, A.A., Ship propellers, *Leningrad (Shipbuilding)(in Russian),* 1988.
8. Nikushchenko D.B. The study of viscous flow of incompressible fluid from the basis of FLUENT, *Lecture note (in Russian), St.Petersburg State Marine Technical University St.Petersburg, Russia*, 2006.
9. Zaw Win and Fridman, G.M. The study of viscous effect on spoiler mounted on the trailing edge of the supercavitating hydrofoil, *SubSeaTech 2009, June 2009, St.Petersburg, Russia*, 2009.
10. Waid, R.L., Lindberg, Z.M. Experimental and Theoretical Investigation of A Supercavitating Hydrofoil, *Report No. 47-8*, *Engineering Division California Institute of technology*, 1957.
11. Kinnas, S.A.& Mazel, C.H., Numerical vs. Experimental Cavitation Tunnel (A supercavitating hydrofoil experiment), *Proceeding of the Twenty-Third American Towing Tank Conference*, 1993, pp, 165-173.
12. Krishnaswamy, P., Andersen, P. and Kinnas, S.A., Re-Entrant Jet Modelling for Partially Cavitating Two-Dimensional Hydrofoils, Fourth International Symposium on Cavitation, CA USA, June 20-23, 2001.
13. Pearce, B.W.& Brandner, P.A., Limitations on 2D Super-cavitating Hydrofoil Performance, *16th Australasian Fluid Mechanics Conference, Crown Plaza, Gold Coast, Australian,*2-7 Dec. 2007.
14. Yasumoto, I. Viccosity of Water Vapor in the Temperature Range from 6°C to 29 °C, *Bulletin of the Chemical of Japan*, Vol. 43, 1970, pp. 3917-3919.
15. Ukon, Y. Research on Design and Application of Supercavitating Propellers, 1996, SRI, vol. 33, No. 3. p. 151-180.
16. Plotkin, A.A., Leading edge correction for supercavitating flat-plate hydrofoil*, Journal of Fluid Engineering, Transactions of A.S.M.E.*, series D, vol. 100, No.3, 1978, pp276-280.